Title
Seasonal performance evaluation of zero-superheat active refrigerant charge control for variable-speed heat pumps

Journal
Energy and Buildings, 351

ISSN
0378-7788

Authors
Guo, Fangzhou
Kim, Donghun
Shen, Bo
et al.

Publication Date
2026

DOI
10.1016/j.enbuild.2025.116663

Energy & Buildings 351 (2026) 116663

Contents lists available at ScienceDirect

Energy & Buildings

journal homepage: www.elsevier.com/locate/enbuild

Seasonal performance evaluation of zero-superheat active refrigerant charge control for variable-speed heat pumps

Fangzhou Guo [a,*], Donghun Kim [a], Bo Shen [b], Philani Hlanze [c], Jie Cai [d]

[a] Building Technology & Urban Systems Division, Lawrence Berkeley National Laboratory, Berkeley, CA, USA
[b] Buildings and Transportation Science Division, Oak Ridge National Laboratory, Oak Ridge, TN, USA
[c] School of Aerospace and Mechanical Engineering, University of Oklahoma, Norman, OK, USA
[d] School of Mechanical Engineering, Purdue University, West Lafayette, IN, USA

ARTICLE INFO

Keywords:
Heat pump
Optimal control
Zero superheat control
Refrigerant charge control
Speed coordination

ABSTRACT

Heat pumps account for a significant portion of electricity consumption in buildings, making their energy efficiency a critical area of research. Control optimization is recognized as an effective approach for enhancing the efficiency of building HVAC systems. Specifically, since the efficiency of heat pumps increases with reduced superheat and the optimal refrigerant charge level varies with operating conditions, zero-superheat active charge control is a promising strategy to maximize the system's COP. However, due to its complexity, this control strategy remains in the research phase and has only been tested under limited operating conditions. This paper proposes a methodology to evaluate the seasonal performance improvement of zero-superheat active charge control across a full range of heating conditions in buildings. The methodology includes the development of an optimal controller that utilizes an accumulator to store excess refrigerant and manages the active charge level at zero superheat through subcooling control, as well as the creation of a detailed physics-based heat pump model. Targeted a 3-ton variable-speed heat pump with R410A refrigerant, we selected ten U.S. cities representing different climate regions for seasonal performance evaluation. Our simulations indicate that, depending on the climate conditions, the optimal control strategy could achieve energy savings ranging from 5.8 % to 8.0 % over the entire heating season. These results suggest that zero-superheat active charge control, combined with coordinated compressor and fan speeds, could substantially improve the energy efficiency of heat pump systems while maintaining the required heating capacity.

1. Introduction

Air conditioners and heat pumps used for cooling, refrigeration, and space heating in buildings account for over 20 % of total electricity consumption in the U.S[1]. In recent decades, researchers have put considerable effort into enhancing the energy efficiency of these systems within building environments. Those efforts include optimizing heat exchanger designs [2–4], improving compressor technologies [5], developing new refrigerants [6–8], adopting predictive maintenance [9–11], and implementing advanced control strategies [12–15]. Among those technologies, optimal control is considered one of the most cost-effective strategies for improving energy efficiency, particularly with the rapid advancements in computing, communication, and sensing technologies. In particular, suction-line superheat and liquid-line subcooling are the two most critical control parameters influencing system efficiency and reliability. This paper aims to analyze a new optimal control strategy for heat pumps termed zero-superheat active refrigerant charge control.

Fig. 1 shows a schematic diagram of the vapor compression cycle for R410A refrigerant with an accumulator. The compressor intakes low-pressure, low-temperature vapor refrigerant and compresses it to high-pressure, high-temperature vapor. The vapor flows into the condenser, where it releases heat to the environment and then condenses into high-pressure liquid. The liquid refrigerant moves to the expansion valve (EXV), where its pressure and temperature are reduced before entering the evaporator. In the evaporator, the two-phase refrigerant absorbs heat and evaporates back into the vapor phase. Except for the four main components, the suction accumulator also plays a crucial role by intercepting liquid refrigerant at suction, ensuring that only vapor enters the compressor, thus preventing potential damage from liquid slugging. The heat pump manufacturers usually recommend a specific refrigerant

* Corresponding author.
E-mail addresses: fzguo@lbl.gov (F. Guo), donghunkim@lbl.gov (D. Kim), shenb@ornl.gov (B. Shen), philanihlanze@ou.edu (P. Hlanze), cai40@purdue.edu (J. Cai).

https://doi.org/10.1016/j.enbuild.2025.116663
Received 8 April 2025; Received in revised form 14 October 2025; Accepted 29 October 2025
Available online 17 November 2025
0378-7788/

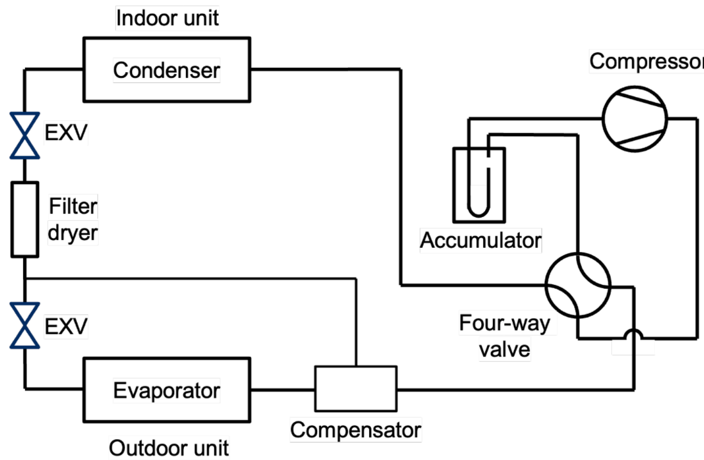

Fig. 1. Schematic diagram of the refrigeration cycle for a heat pump.

Nomenclature

Physical parameters

C_d	Degradation coefficient
f_{comp}	Compressor speed
$f_{nominal}$	Nominal compressor speed
$Q_{cap,des}$	Design capacity [W]
Q_{cap}	Heating capacity [W]
Q_{load}	Heating load [W]
T_{bal}	Balancing dry-bulb temperature [°C]
$T_{hdb,des}$	Heating dry-bulb design temperature [°C]
T_i	Indoor temperature [°C]
T_o	Outdoor temperature [°C]
T_{sc}	Liquid-line subcooling temperature [K (Kelvin)]
UA	Thermal capacitance of the house [W/k]
V_s	Indoor fan volume flow rate [m^3/s]
V_{rate}	Rated indoor fan volume flow rate [m^3/s]
W_{fan}	Indoor fan power [W]
W_{tot}	Total power consumption [W]
$\bar{W}_{tot}$	Time-average power during the cycling period [W]

Abbreviations

COP	Coefficient of performance
EIR	Energy input ratio
EXV	Expansion valve
HPDM	Heat pump design model
HVAC	Heating, ventilation, and air conditioning
MAPE	Mean absolute percentage error
RMSE	Root mean square error
TMY	Typical meteorological year
PLR	Part load ratio
PLF	Part load fraction

charge for system installation. However, this static charge value might not ensure optimal system efficiency across all operating conditions. For heat pumps equipped with an accumulator, system efficiency can be enhanced by adjusting the “active charge”, which is the refrigerant actively circulating in the vapor compression cycle. More specifically, the active charge is the refrigerant inside the compressor, condenser, and evaporator, but does not include the refrigerant in the accumulator or compensator. The active charge can be decreased by opening the EXV under zero-superheat conditions, causing liquid refrigerant to accumulate in the suction accumulator. Conversely, it can be increased by closing the EXV, which reduces the liquid refrigerant level in the accumulator under the same conditions. Thus, by modulating the EXV opening under zero-superheat conditions, the amount of liquid refrigerant in the suction accumulator can be controlled.

Fig. 2 demonstrates the changes in suction-line superheat, liquid-line subcooling, active refrigerant charge, and COP as the EXV opening gradually increases for R410A refrigerant. In this example, the EXV steps range from 0 (fully closed) to 500 (fully open). As the EXV step increases, the mass flow rate in the evaporator rises, resulting in a decrease in the superheat. When the EXV step reaches 170 (34 % open), the superheat level drops to zero. Meanwhile, subcooling also decreases gradually. At zero superheat, liquid refrigerant begins to accumulate in the suction accumulator, not actively circulating in the heat pump cycle. As the EXV opening continues to increase, more liquid refrigerant accumulates in the accumulator, which further reduces the active charge level in the system. The EXV opening affects the COP by adjusting the pressure difference across the EXV, the isentropic efficiency of the compressor, and consequently, the compressor power. In this scenario, the maximum COP is achieved at an EXV opening of 210 (42 % open), which is 12.8 % higher than the baseline at 5 K superheat. Since the superheat is maintained at approximately 0 K in active charge management, it cannot be used to adjust the EXV opening. However, as shown in Fig. 2(a), the subcooling level has a monotonic decreasing relationship with the EXV opening, making subcooling a suitable control variable. Therefore, in zero-superheat active charge control, the EXV control strategy is shifted from targeting a specific superheat level (e.g., 5 K) to targeting an optimal subcooling level. The heating capacity is also influenced by the EXV opening. However, the change in heating capacity varies with operating conditions, depending on the overall heat transfer coefficient and the temperature difference between the refrigerant and air at the condenser. For variable-speed heat pumps, the additional degrees of freedom provided by the variable-speed compressor and indoor fan create an opportunity to further enhance efficiency while meeting a given heating load. Therefore, to maintain the heating capacity and maximize the system efficiency, the zero-superheat active charge control could be combined with optimized coordination of compressor and fan speeds.

Although zero-superheat active charge control can significantly increase the COP of heat pumps with no hardware upgrade, it has not been implemented in real systems due to several practical challenges. These challenges include the complexity of control algorithms, maintaining control stability at zero superheat, and the risk of liquid refrigerant entering the compressor [16–18]. However, advancements in manufacturing, computing, communication, and sensing technologies are making zero-superheat active charge control more feasible. For instance, modern compressors, such as scroll compressors, are more tolerant of wet compression. Also, though there could be small oscillations in superheat when it is close to zero, we observed that in the active charge control,

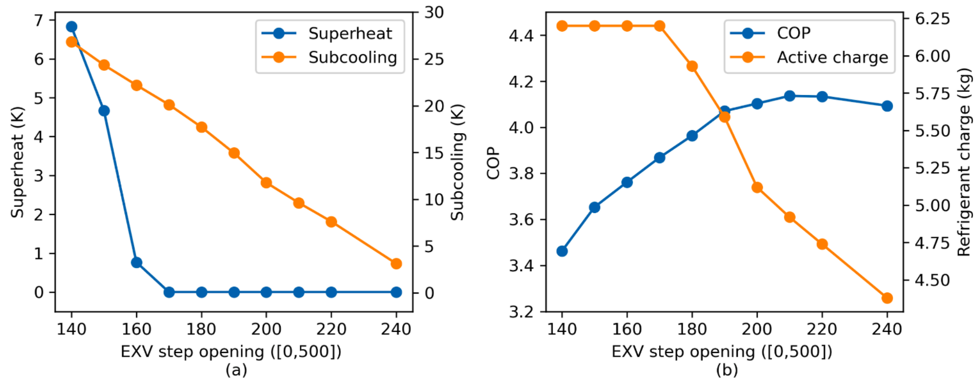

Fig. 2. Experimental demonstration of heat pump performance at zero superheat (refrigerant: R410A).

the quality at the evaporator outlet is slightly below one, away from the regimes with superheat oscillations.

Although limited, some studies in the literature have focused on active charge management using either a receiver or an accumulator to store excess refrigerant. For example, Kim and Braun (2012) [17] used accumulators to modify system charges and experimentally evaluated the impact of charge levels on system efficiency. To prevent the accumulator from being completely filled during zero-superheat control, Liu and Cai (2022) [19] proposed a liquid-level estimator for the accumulator and demonstrated its accuracy through both simulation and experiment for a heat pump. Jensen and Skogestad (2007) [18] investigated the benefits of using a receiver and a control valve in the refrigeration cycle to manage excess refrigerant and optimize subcooling. Their results indicated that maximum efficiency could be achieved at a specific subcooling level, emphasizing the importance of managing the refrigerant charge for improved system performance. Menken et al. (2014) [20] compared the performance of using an accumulator versus a receiver for active charge management for a heat pump. They found that the system with a receiver had a higher COP, but the system with an accumulator could be preferable in a cold climate. Plus, the zero-superheat level is automatically satisfied by using an accumulator to store the liquid refrigerant, which is a significant advantage. Besides, some studies designed or evaluated active charge controllers. Koeln and Alleyne (2014) [21] used a receiver and an additional EXV to provide independent control of the subcooling, and showed that there is an optimal subcooling level that maximizes system efficiency, which varies with operating conditions. They also implemented extremum seeking control (ESC) to identify the optimal subcooling and showed a 9 % performance enhancement. Moreover, some researchers also studied the speed coordination of heat pumps. Fischer and Rice (1985) [22] designed a heat pump model to minimize its annual energy consumption by finding the optimal fan speed. Zakula et al. (2012) [23] designed an optimization algorithm to find the optimal coordination of evaporator airflow, condenser airflow, and subcooling for which the total power consumption is minimal at a given operation condition, and the optimization is based on a static heat pump model.

From the literature review, very few researchers have investigated active charge control. Moreover, they demonstrated the efficiency gain of active charge control through experiments, which could only test a limited number of operating conditions and could not cover the full range of possible scenarios. Therefore, the overall efficiency gain of the heat pump throughout the entire heating season is still unknown under a specific climate. Additionally, there is currently no control algorithm for active charge management in the industry. Based on these research gaps, this study contributes to zero-superheat active charge control as follows:

- Proposed a methodology to evaluate the seasonal performance of zero-superheat active charge control. The methodology is applied to assess the seasonal energy savings of this control strategy for small residential buildings across a full range of heating operating conditions in ten U.S. cities in different climate regions.
- Developed a model-based optimal controller that uses the accumulator to manage the active charge level at zero superheat in the heat pump. The optimal controller also coordinates the compressor and fan speeds to achieve the maximum COP while meeting the required heating load.
- Developed a detailed physics-based heat pump model to simulate and compare the performance of the active charge control with a baseline representing the conventional control strategy.

The novelty of this study lies in the comprehensive approach to evaluating the seasonal performance of zero-superheat active charge control and a detailed analysis of the control algorithm's efficiency gains. Compared with previous research, the proposed control algorithm offers a more efficient solution for heat pump control, with significant potential for energy savings in small residential buildings.

2. Methodology

This section first outlines the methodology used to evaluate the seasonal performance of zero-superheat active charge control for residential heat pumps under heating conditions. Then, Sections 3.2 and 2.3 introduce the development of the high-fidelity heat pump design model (HPDM) and the control-oriented reduced order models, respectively. Using the reduced order models, an optimal control problem is formulated to minimize total power consumption within specified bounds for the control variables in Section 2.4.

2.1. Introduction to the seasonal performance evaluation process

Fig. 3 shows the framework to evaluate the seasonal performance of zero-superheat active charge control. Given the location of a residential building where the heat pump is installed, its typical meteorological year (TMY) weather data and heating dry-bulb design temperature are retrieved first. The heating dry-bulb design temperature is used for system sizing, and the hourly heating load is calculated using the system sizing information and the hourly weather data. Then, the optimal control algorithm searches for the minimum power of the heat pump in each operating hour by adjusting the control variables (i.e., the indoor fan speed, compressor speed, and liquid-line subcooling) while ensuring the heating capacity matches the required heating load. After that, a high-fidelity heat pump model (HPDM) takes the optimal control variables and the weather data as inputs to compute the heating power, heating capacity, COP, and other physical properties in the refrigeration cycle. On the other hand, a baseline controller is created for comparison, which assumes a controlled suction-line superheat of 5 K, fixed active charge level (i.e., no liquid refrigerant inside the accumulator), and synchronized compressor and indoor fan speeds to meet the required heating

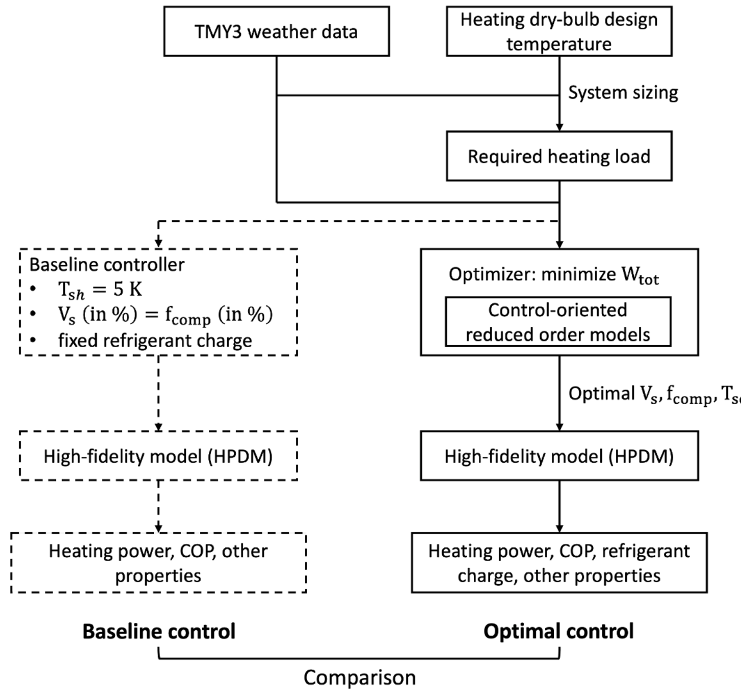

Fig. 3. Framework of the seasonal performance evaluation process.

load. Finally, the energy efficiency and physical properties between the optimal control and the baseline are compared, and the advantages of the optimal control are analyzed.

2.2. Development of a high-fidelity heat pump model

A high-fidelity heat pump model has been developed and calibrated from data collected for a 3-ton residential heat pump with R410A refrigerant in a research lab. The model employs the Heat Pump Design Model (HPDM) [24], a building equipment modeling platform created by the Oak Ridge National Laboratory for steady-state and quasi-steady-state design analyses of extensive thermal system configurations. In HPDM, each piece of equipment is modeled separately. The compressor model is constructed using the AHRI compressor maps [25]. Two heat exchangers are modeled using the finite control volume approach, which discretizes a heat exchanger into multiple segments and then calculates local heat transfer and pressure drop in each segment. The fan models are created by fitting a function to the relationship between power consumption and air flow rate.

2.3. Development of control-oriented reduced order models

To be shown in Fig. 6 (Section 3.3), the high-fidelity model is very accurate after calibration, and can be used for simulating the heat pump performance in varying operating conditions. However, because it is a complex and detailed model which requires significant computational resources, the model is impractical for real-time control and optimization tasks. Therefore, there is a need to develop control-oriented reduced order models based on the high-fidelity model simulation results. These simplified models can capture the essential characteristics of the system while being computationally efficient, making it suitable for model-based optimization.

The proposed optimal controller needs three reduced order models:

1. The heating capacity (Q_{cap}) is modeled as a function of the indoor fan volume flow rate (V_s), compressor speed (f_{comp}), indoor temperature (T_i), outdoor temperature (T_o), and liquid-line subcooling temperature (T_{sc}). This model structure is based on the ASHRAE Toolkit model [26], but accounts for additional correction terms associated with compressor speed and subcooling.

$$\begin{aligned} Q_{cap} =& (a_0 + a_1 T_i + a_2 T_o + a_3 T_i^2 + a_4 T_o^2 + a_5 T_i T_o) \\ & \cdot (1 + a_6 \frac{V_s}{V_{rate}} + a_7 (\frac{V_s}{V_{rate}})^2) \\ & \cdot (1 + a_8 f_{comp} + a_9 f_{comp}^2 + a_{10} f_{comp}^3) \\ & \cdot (1 + a_{11} T_{sc} + a_{12} T_{sc}^2) \end{aligned} \tag{1}$$

2. The compressor energy input ratio (EIR) is also modeled as a function of the indoor fan volume flow rate (V_s), compressor speed (f_{comp}), indoor temperature (T_i), outdoor temperature (T_o), and liquid-line subcooling temperature (T_{sc}). Since the ASHRAE Toolkit model structure shows a relatively high prediction error, an artificial neural network (ANN) model is used. The ANN model has two hidden layers, each with 32 neurons.

$$EIR = f_{\mathrm{ANN}}(T_i, T_o, V_s, f_{comp}, T_{sc}) \tag{2}$$

3. Modeling the indoor fan power (W_{fan}) as a cubic function of its volume flow rate (V_s).

$$W_{fan} = b_0 + b_1 \frac{V_s}{V_{rate}} + b_2 (\frac{V_s}{V_{rate}})^2 + b_3 (\frac{V_s}{V_{rate}})^3 \tag{3}$$

With the above three models, the total power consumption (W_{tot}) of the heat pump system can be calculated by:

$$W_{tot} = W_{fan} + EIR \cdot Q_{cap} \tag{4}$$

2.4. Formulation of an optimal control problem

The optimal controller designed in this study is a combination of the zero-superheat active charge controller and the fan-compressor speed coordination controller. The control variables include the setpoint of the subcooling temperature (T_{sc}), the indoor fan volume flow rate (V_s), and the compressor speed (f_{comp}). The outdoor fan speed is fixed. The goal of the optimal controller is to find the optimal control setpoint for the heat pump to minimize the total power consumption while ensuring the

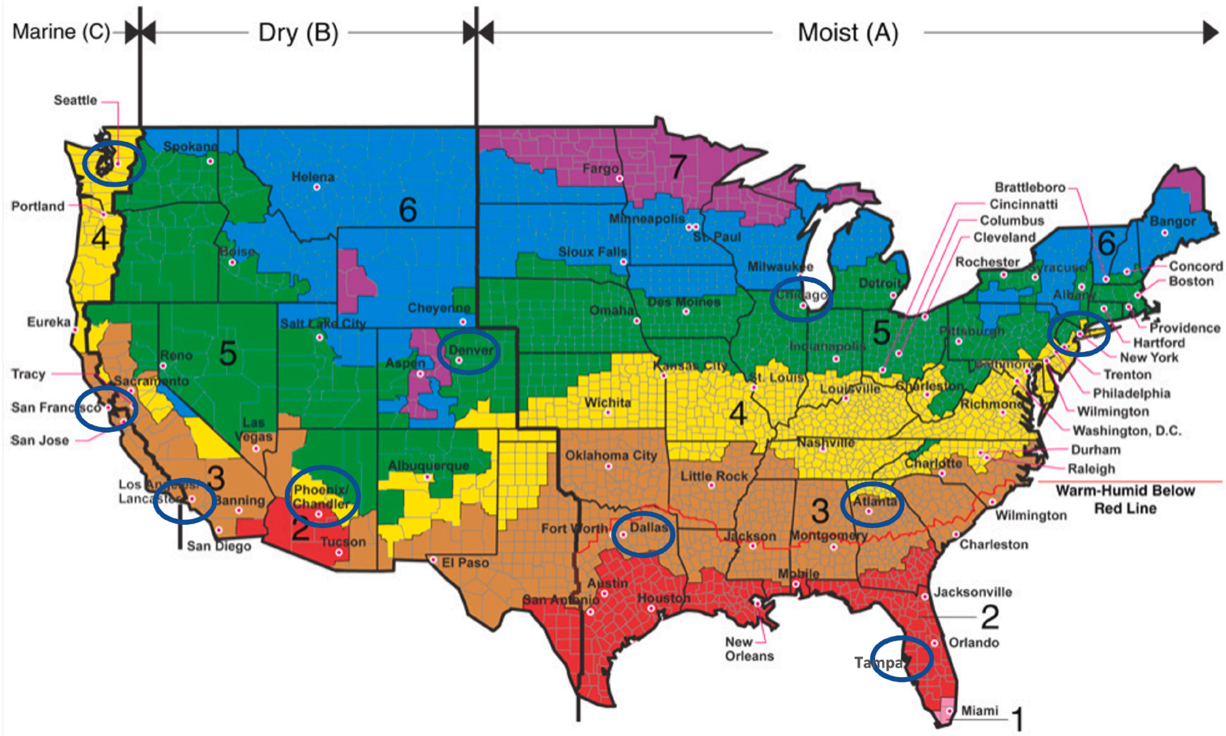

Fig. 4. Selected cities for simulation in this study.

required heating load is met. This can be formulated into a constrained optimization problem. The control objective is:

$$\min_{V_s, f_{comp}, T_{sc}} W_{tot} \tag{5}$$

while the constraint is that the heating capacity should equal the heating load:

$$Q_{cap} = Q_{load} \tag{6}$$

and each control variable is bounded:

$$0.5 < \frac{V_s}{V_{rate}} < 1 \tag{7}$$

$$0.3 < \frac{f_{comp}}{f_{nominal}} < 1 \tag{8}$$

$$1\ \text{K} < T_{sc} < 15\ \text{K} \tag{9}$$

The upper bounds for the compressor and fan speeds correspond to their nominal speeds, while the lower bounds are set to 30 % and 50 % of their nominal speeds, respectively, in accordance with the manufacturer's specifications and the operational stability requirements of the heat pump unit. For subcooling, the lower bound is set at 1 K, which means the condenser basically has no subcooling. The upper bound is set at 15 K, since a very long subcooling region in the condenser degrades the total heat transfer efficiency, which is not favorable.

3. Simulation setup

The simulation is performed based on a real 3-ton variable-speed heat pump unit. The manufacturer-suggested refrigerant charge level is 6.2 kg of R410A. In the heating mode, about 0.7 kg of refrigerant is stored inside the compensator. Thus, if the accumulator is empty, the active charge in the refrigeration cycle is about 5.5 kg. The nominal compressor speed is 5000 rpm, and the rated indoor fan volume flow rate is 0.566 m^3/s (1200 CFM, tested in the psychrometric chamber). This section will detail the setup of the simulation, including selecting 10 locations for simulation, calculating the hourly heating load in each location, training and calibration of the simulation models, and design details of the baseline and optimal controllers.

3.1. Selection of locations for simulation

This study selected 10 cities in the U.S.A. to perform the simulation. As shown in Fig. 4, the cities are selected based on the International Energy Conservation Code (IECC) climate zones and moisture regimes [27]. Because this study only analyzed the heating conditions of the heat pump, cities in the Climate Zone 1 are not selected. Also, cities in Climate Zones 6 and 7 are too cold for the current heat pump to operate. For future work, a model for the cold climate heat pump could be developed to test the performance in those very cold cities. Table 1 lists the 10 selected cities along with their heating or cooling dry-bulb design temperature.

3.2. Calculation of the hourly heating load

For each selected city, its hourly outdoor air temperature in the whole year can be retrieved from the typical meteorological year (TMY) weather data. However, in order to evaluate the heat pump performance at different operating conditions, the hourly heating load should also be specified in addition to the outdoor air temperature data. In this study, the hourly heating load of a heating-dominant location is determined by a system sizing method with the following three steps:

1. The design capacity ($Q_{cap,des}$) of the heat pump is calculated at the heating dry-bulb design temperature ($T_{hdb,des}$) of the location and an indoor temperature of 70°F (21.1 °C), assuming the indoor fan and compressor operating at full speeds, the subcooling set at 10 K, and the heat pump unit oversized by 20 %:

$$(1+20\,\%)\cdot Q_{cap,des} = f_Q(T_i = 21.1\,°\text{C}, T_o = T_{hdb,des}, V_s = V_{rate}, f_{comp} = f_{nominal}, T_{sc} = 10\ \text{K}) \tag{10}$$

where f_Q refers to the reduced-order model to predict the heating capacity (Eq. (1)), and the heating dry-bulb design temperature

Table 1
IECC climate zones of the selected cities for simulation.

Climate zone	City	Heating dry-bulb design temperature	Cooling dry-bulb design temperature	Note
2A	Tampa	3.6 °C	33.6 °C	Cooling dominant
2B	Phoenix	3.7 °C	43.4 °C	Cooling dominant
3A	Dallas	−6.5 °C	38.0 °C	Heating dominant
3A	Atlanta	−6.3 °C	34.3 °C	Heating dominant
3B	Los Angeles	6.9 °C	28.7 °C	Cooling dominant
3C	San Francisco	3.8 °C	28.3 °C	Heating dominant
4A	New York	−10.7 °C	32.1 °C	Heating dominant
4C	Seattle	−4.2 °C	29.4 °C	Heating dominant
5A	Chicago	−20.0 °C	33.3 °C	Heating dominant
5B	Denver	−17.4 °C	34.6 °C	Heating dominant

($T_{hdb,des}$) is defined as an extreme temperature that occurs for 0.4 % of the year. An oversizing factor of 20 % ensures that the heating load can be met in extremely cold weather and also during the time when the heat pump runs continuously to track an increased thermostat heating setpoint.

2. Then, consider a house with its room temperature controlled by the heat pump. The thermal resistance of the house ($1/UA$) is calculated by:

$$\frac{1}{UA} = \frac{T_{bal} - T_{hdb,des}}{Q_{cap,des}} \tag{11}$$

where T_{bal} is the balancing dry-bulb temperature, an ideal outdoor temperature where no heating or cooling is required for that house. The balancing temperature is set at 65°F (18.3 °C) in this study. Note that the balancing temperature should be lower than the indoor temperature at zero load, considering the internal heat gains in the house.

3. Finally, the heating load (Q_{load}) in each hour can be calculated by:

$$Q_{load} = UA \cdot (T_{bal} - T_o) \tag{12}$$

where T_o is the outdoor temperature data retrieved from the TMY weather dataset.

Similarly, for cooling-dominant locations, the system is sized based on the cooling dry-bulb design temperature, following the same three steps. For the 10 selected cities, Tampa, Phoenix, and Los Angeles are cooling-dominant cities, and the others are heating-dominant cities.

3.3. Model calibration

The development and calibration process of the simulation models is shown in Fig. 5. First of all, some experimental data on the heat pump are collected to calibrate the high-fidelity model. Then, the calibrated high-fidelity model generates thousands of simulation data points at zero superheat but with different operating conditions. Finally, the control-oriented reduced-order models are trained and validated using the simulation dataset.

Table 2 shows the specifications of the heat pump system in this study. In order to collect experimental data for validation of the high-fidelity model, three sets of experimental tests were performed, as shown in Table 3. First of all, Test #1 focused on operations at normal superheat levels (i.e., 5 °C), and the total charge level varied from 5 kg to 6.2 kg. Then, Test #2 and #3 focused on zero-superheat conditions. Test #2 varied the EXV steps from 140 to 240, while other variables are fixed. In this process, the superheat gradually decreased to zero and the refrigerant started to accumulate in the accumulator. In Test #3, this process was repeated but at different levels of compressor speed, fan speed, and outdoor temperature.

Fig. 6 shows the calibration results of the high-fidelity heat pump model in heating mode, with the x-axis representing experimental data and the y-axis representing the model simulation results. The experimental data were collected at various EXV openings and refrigerant charge levels under H1 and H2 testing conditions, as specified by the AHRI Standard 210/240 [28]. The high-fidelity model demonstrates high accuracy in predicting heating capacity, power consumption, and COP, with a mean absolute percentage error (MAPE) of less than 2 %. Additionally, the model accurately predicts the refrigerant charge level, achieving an MAPE of 3.5 %. It is important to note that the charge level prediction is used solely for validation and does not influence the control and optimization process or the calculation of efficiency gains.

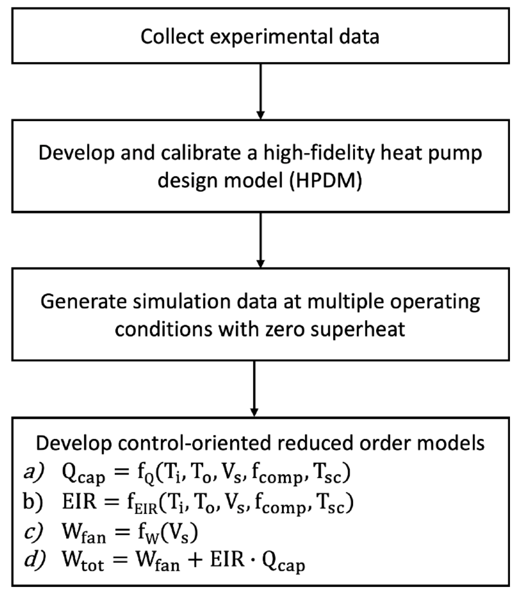

Fig. 5. Process to develop high-fidelity and control-oriented simulation models.

A large amount of data is generated from the calibrated high-fidelity model to train and validate Eqs. (1) and (2) of the reduced-order models, while Eq. (3) is directly fitted using experimental test data as it has fewer coefficients. As shown in Table 4, each input variable of the reduced order models spans a wide range of heat pump operating conditions. Then, the large dataset is split into a training set and a validation set. Fig. 7(a) and (b) display the validation results of the reduced-order models after training. The predictions of the high-fidelity model and the reduced-order models agree well, with the MAPE for heating capacity at 1.1 % and for EIR at 1.0 %. Fig. 7(c) compares the fitted indoor fan curve with experimental data, showing that the prediction error for indoor fan power is also very low.

3.4. Design of the optimal controller

Based on the optimization problem formulated in Section 2.4, an algorithm is developed to determine the optimal control setpoint for each hour. With only three control dimensions (i.e., indoor fan airflow rate V_s, compressor speed f_{comp}, and liquid-line subcooling temperature T_{sc}) and clearly defined bounds for each variable, the brute-force method proves to be both straightforward and efficient. Its computational load is

Table 2
Specifications of the heat pump system.

Parameter	Specification
Tonnage	3
Compressor type	Scroll
Compressor configuration	Modulating
Indoor fan motor	Variable-speed electronically commutated motor
Rated indoor airflow	1200 CFM (0.566 m^3/s)
Seasonal Energy Efficiency Ratio (SEER)	20

Table 3
Experimental data collection for validation of the high-fidelity model.

Test	f_{comp}	V_s	EXV steps	T_i	T_o	Total charge
#1	3200 rpm	0.566 m^3/s	–	21.1 °C	8.3 °C	5~6.2 kg
#2	3200 rpm	0.566 m^3/s	140~240	21.1 °C	8.3 °C	6.2 kg
#3	1300~3000 rpm	0.226~0.566 m^3/s	100~170	21.1 °C	1.4 °C~12.5 °C	6.2 kg

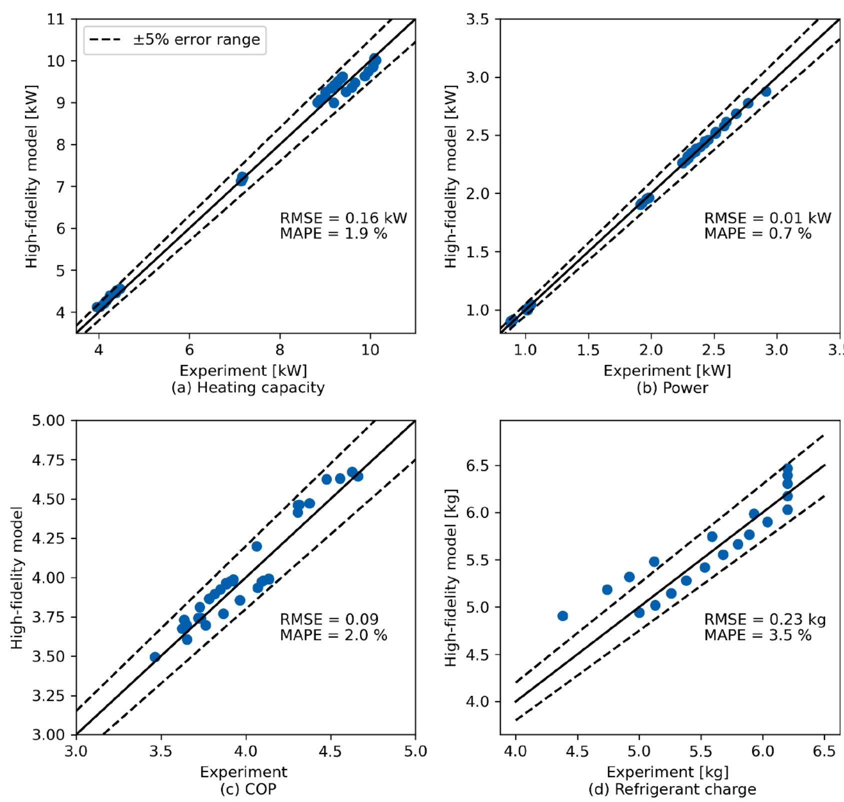

Fig. 6. Validation of the high-fidelity model (HPDM).

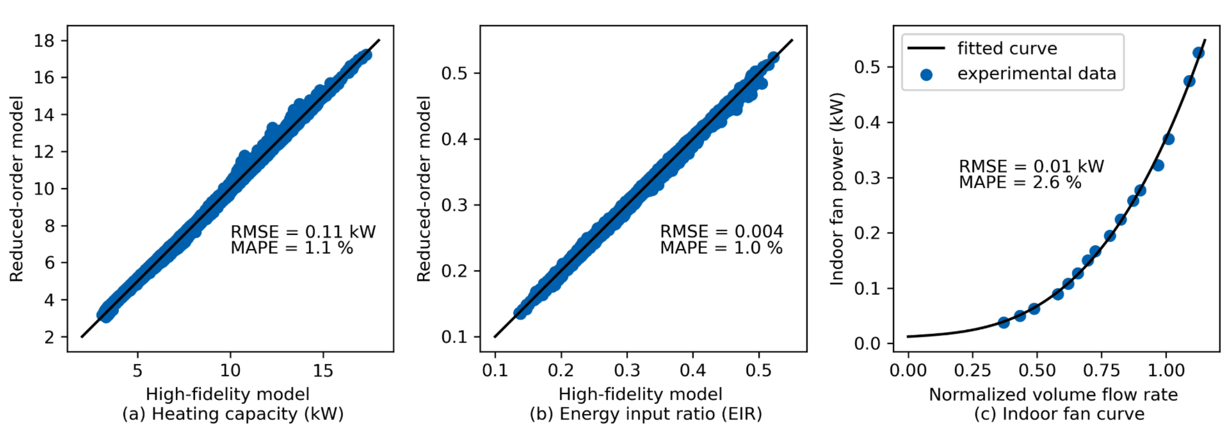

Fig. 7. Validation of the control-oriented reduced order models.

Algorithm 1 An algorithm to find the optimal control setpoint.

for *hour* = *September 1st 00:00* to *June 1st 00:00* **do**
  if $Q_{load} = 0$ **then**
    continue to the next iteration
  end if
  Generate a DataFrame X having all combinations of V_s, f_{comp}, and T_{sc} with small increment
  Predict Q_{cap} and W_{tot} for X using the reduced-order models at $T_i = 21.1$°C and current T_o
  Store the predictions in two DataFrames Y_1 and Y_2
  Filter Y_1 to include only rows where $|Q_{cap} - Q_{load}| < 0.02$kW
  Assuming $PLR = 1$, calculate $\bar{W}_{tot}$ for every row of Y_1
  Filter Y_2 to include only rows where $Q_{cap} - Q_{load} > 0.02$kW
  Assuming $PLR < 1$, calculate $\bar{W}_{tot}$ for every row of Y_2 using Eqs. (13)–(15)
  Concatenate Y_1 and Y_2 into a single DataFrame Y
  Select the row in Y with the minimum $\bar{W}_{tot}$
end for

Table 4
Data generation from the high-fidelity model: range of the input variables.

Variable	Min	Max	Increasing step
V_s	$0.5 \cdot V_{rate}$	$1.0 \cdot V_{rate}$	$0.1 \cdot V_{rate}$
f_{comp}	$0.3 \cdot f_{nominal}$	$1.0 \cdot f_{nominal}$	$0.1 \cdot f_{nominal}$
T_{sc}	2.8 K (5 R)	22.2 K (40 R)	2.8 K (5 R)
T_i	15.6 °C (60°F)	21.1 °C (70°F)	1.1 °C (2°F)
T_o	−15 °C (5°F)	18.3 °C (65°F)	2.8 °C (5°F)

Table 5
Seasonal energy savings of the heat pump in the heating mode by adopting the optimal control.

City	Energy savings	City	Energy savings
Tampa	7.4 %	San Francisco	7.8 %
Phoenix	7.0 %	New York	5.9 %
Dallas	6.3 %	Seattle	7.0 %
Atlanta	5.8 %	Chicago	6.4 %
Los Angeles	8.0 %	Denver	6.1 %

very low, allowing the algorithm to quickly identify the optimal control point that minimizes power consumption for each operating condition, which makes the brute-force method highly suitable for real-time implementation. The pseudo-code for the brute-force searching algorithm is presented in Algorithm 1.

Additionally, depending on the heating load value, the heat pump may operate continuously or cycle on and off. In this study, the heat pump is considered to be cycling when the compressor operates at the minimum speed, but the heating load is still lower than the heating capacity. The cycling loss is estimated based on a correlation provided in the EnergyPlus Engineering Reference [29]:

$$PLR = \frac{Q_{load}}{Q_{cap}} \tag{13}$$

$$PLF = 1 - C_d + C_d \cdot PLR \tag{14}$$

$$\bar{W}_{tot} = \frac{PLR}{PLF} \cdot W_{tot} \tag{15}$$

where $\bar{W}_{tot}$ refers to the time average power during the cycling period. PLR and PLF refer to part load ratio and part load fraction, respectively. C_d is called the degradation coefficient, which is typically between 0.05 (lower cycling loss) and 0.25 (higher cycling loss) [30]. In this simulation, because the variable-speed heat pump only starts cycling at low compressor speeds, a C_d value of 0.25 is used.

After obtaining the optimal control setpoints for each hour, the heat pump performance is simulated using the high-fidelity model. Fig. 8 shows the control loop for the heat pump by using the optimal controller. Based on T_i, T_o, and Q_{load}, the optimal controller finds out the optimal set for V_s, f_{comp}, and T_{sc}, which are then used to control the operation of the indoor fan, the compressor, and the EXV. The outdoor fan is maintained at a constant speed. Finally, based on the simulation results of the high-fidelity model, the next section will analyze the energy-saving potential by adopting the optimal controller.

3.5. Design of the baseline controller

To quantify the efficiency gain from adopting the optimal controller, we also developed a baseline controller to simulate the control strategy commonly used for heat pumps in the industry. In the baseline, the suction-line superheat is controlled instead of the liquid-line subcooling. We assume a controlled superheat of 5 K and synchronized speeds for the compressor and the indoor fan. Since the superheat is positive, liquid refrigerant will not appear in the accumulator, so the active charge of the refrigeration cycle is nearly constant. In the simulation, the active charge level is assumed to be 5.3 kg. The performance of the baseline controller is also simulated using the high-fidelity model.

4. Results and discussion

4.1. Energy saving potential of each city

Fig. 9 shows the total heating demand and electricity use for each of the 10 locations under the baseline and the optimal control. The heating demand is calculated based on the weather information and the building size in each location (see Section 3.2). Table 5 shows the heating energy savings of the heat pump when the optimal controller is used in place of the baseline controller. The energy savings range from 5.8 % to 8.0 % across different locations, with larger percentages of energy savings achieved in milder locations. Additionally, Fig. 10 compares the heat pump COP under the baseline and optimal control strategy for all locations using a box plot. For most of the time, the heat pump operated under the optimal controller has a higher COP value than under the baseline controller. The next subsection will select two representative cities to show their energy use over time, along with some basic climatic data and the control decisions.

4.2. Case studies

Fig. 11 shows the climatic data, heating demand, energy use, and control variables for the heat pump in Chicago, a typical heating-dominant location in climate region 5A. Based on the TMY3 weather dataset, the daily average outdoor temperature in Chicago is between -20 °C and 30 °C. Fig. 11(b) shows the daily heating demand of the residential building, where relatively heavy heating demands appear between November and April. Fig. 11(c) compares the daily energy usage between the baseline and the optimal control. The optimal controller uses less energy than the baseline controller on each day. Figs. 11(d) to

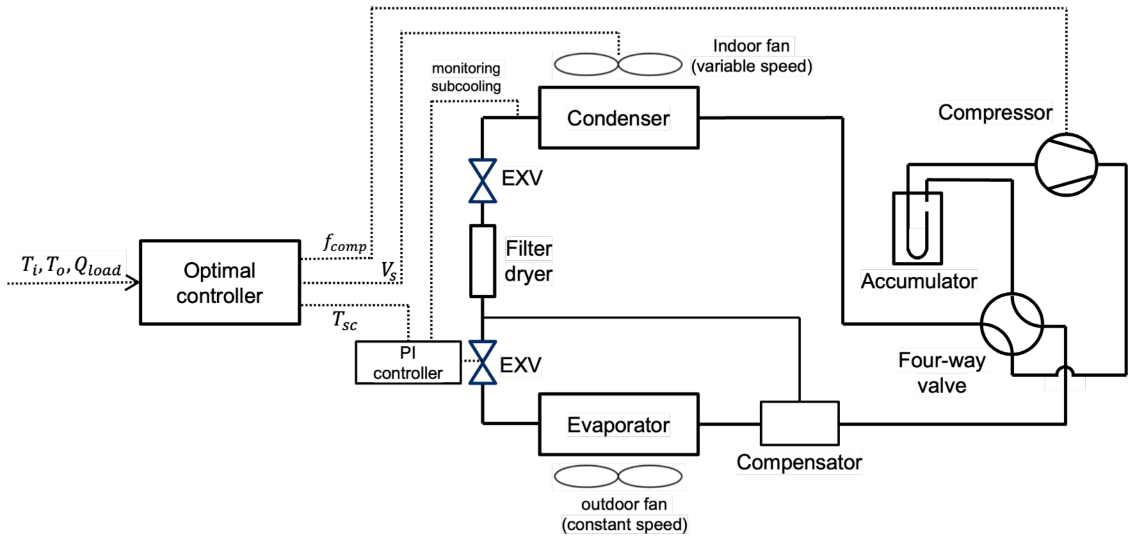

Fig. 8. Schematic diagram of the control loop for the residential heat pump system.

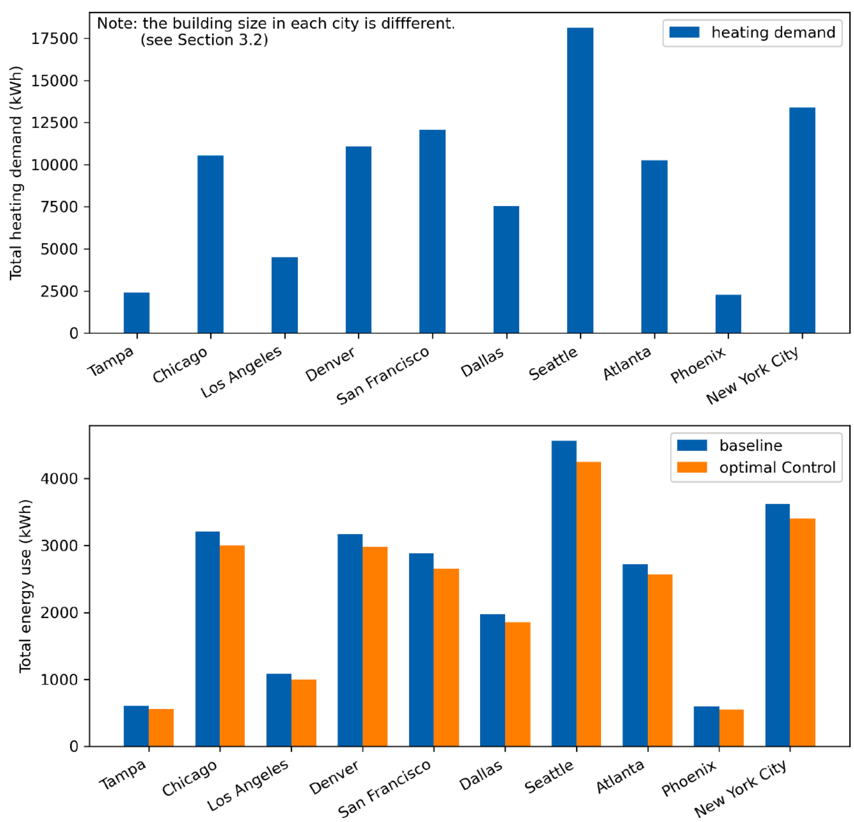

Fig. 9. Total heating demand and energy usage under the baseline and optimal control strategy for all cities.

(f) present the control decisions (the fan and compressor speeds are daily averaged values). Compared to the baseline, the optimal control has a little bit lower compressor speed, but a higher fan speed in general. This is because the fan power is much smaller than the compressor power. Thus, raising the fan speed from 50 % to 60 % minimally increases fan power, but the increased airflow further lowers the condensing pressure, leading to a greater reduction in compressor power. Additionally, the optimal control consistently maintains a lower subcooling temperature.

Fig. 12 compares the same features in Los Angeles (climate region 3B, cooling-dominant location). Unlike the situation in Chicago, the heating load in Los Angeles is much lower than its cooling load, and the compressor generally operates at a lower part-load ratio. Nevertheless, the optimal control achieves an overall energy savings of 8.0 %, which remains highly beneficial for practical applications. The next subsection will explore the reasons behind the energy savings by analyzing the physical properties of the refrigeration cycle under the two control strategies.

4.3. Analysis of simulation results

Fig. 13 illustrates the vapor compression cycle under the two control strategies in a P-h diagram. In this example, the outdoor temperature is 0 °C, the indoor temperature is 21.1 °C, and the heating load is 2.7 kW.

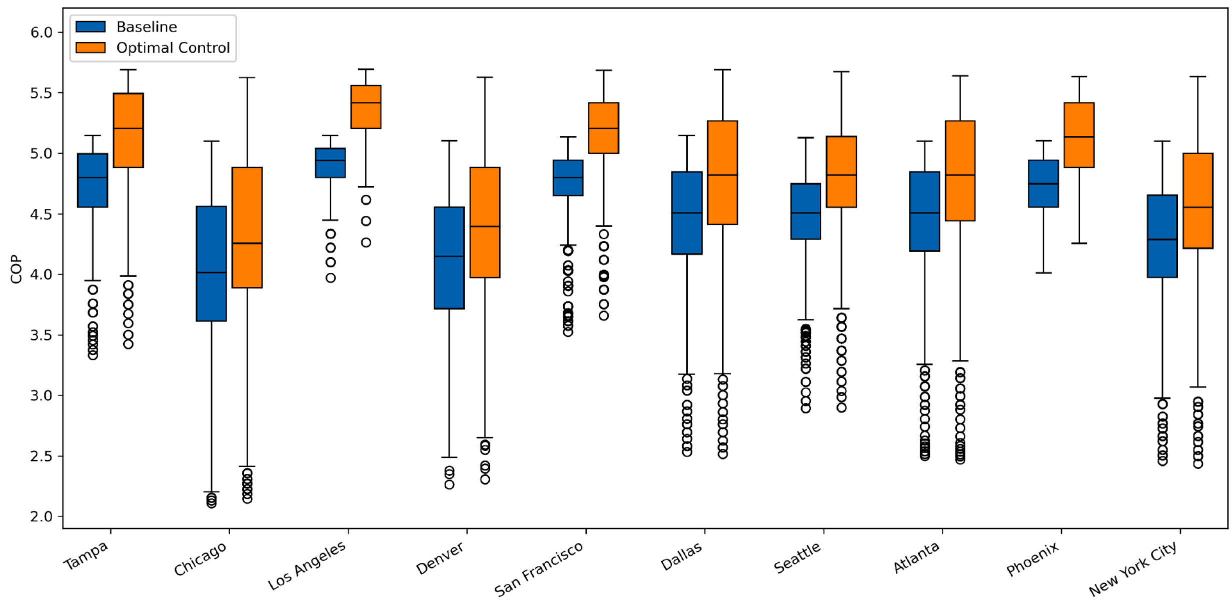

Fig. 10. Heat pump COP under the baseline and optimal control strategy for all cities.

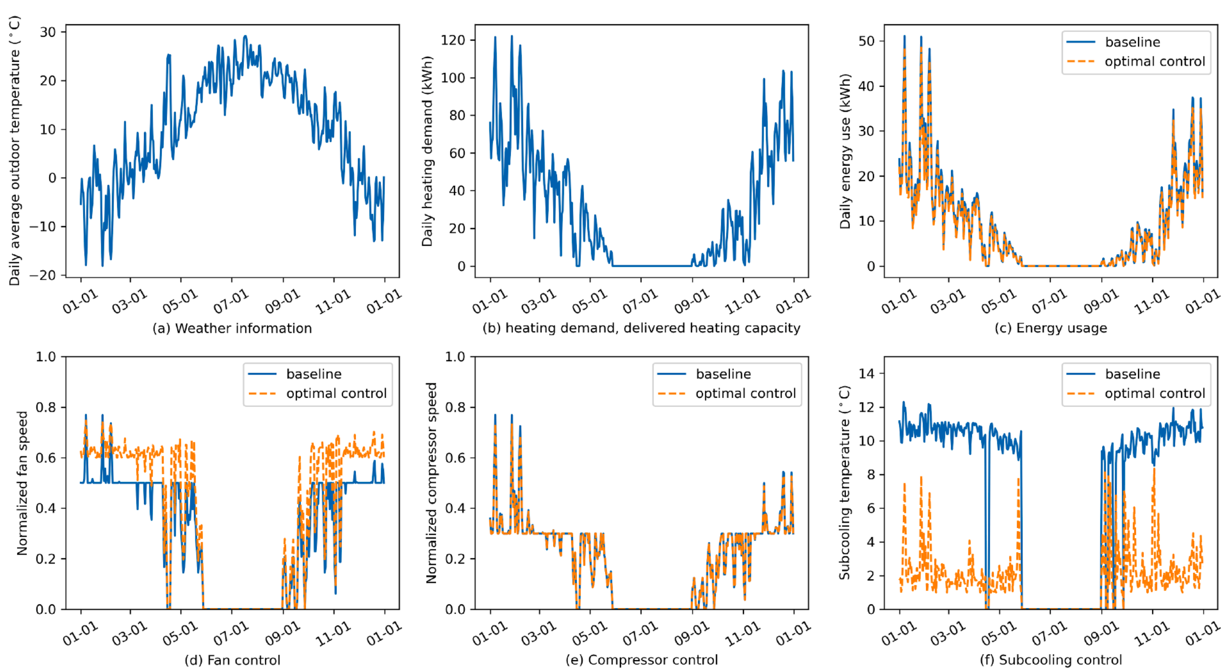

Fig. 11. Weather, heating demand, energy use, and control variables for the heat pump in Chicago over time.

The heat pump is cycling with a duty factor of approximately 80 % under both controls. The cycle in blue is the baseline control, where the superheat is controlled at 5 K and the subcooling is 11.0 K. The cycle in orange results from the optimal control, where the superheat is around 0 K and the subcooling is controlled at 1 K. The EXV opening in the optimal control is larger, and its refrigerant mass flow rate is higher than the baseline. From the diagram, the optimal control has a higher COP due to the following reasons:

- **Much lower condensing pressure and temperature.** Under optimal control, the subcooled region and the superheated vapor region in the condenser are both shorter, resulting in a higher total heat transfer coefficient on the refrigerant side. Note that for R410A, the heat transfer coefficient of the saturated mixture is significantly higher than that of the single phase. Additionally, the optimal control has a higher refrigerant mass flow rate, which further improves the refrigerant side heat transfer. Together, these two factors allow the condenser to achieve the same amount of heat transfer at a lower condensing temperature, thereby enhancing system efficiency.
- **Higher evaporating pressure and temperature.** Similarly, in the optimal control, the superheated vapor region in the evaporator is replaced by the two-phase region, which has a higher heat transfer coefficient. Combined with the fact that the refrigerant mass flow rate is also higher, the increase in the overall heat transfer coefficient allows the refrigerant to absorb heat at a higher evaporating temperature and pressure.
- **Lower compression pressure ratio.** Because the optimal control has a higher evaporating pressure and a lower condensing pressure, its compression pressure ratio is much lower. Therefore, the compressor consumes much less energy to provide the same heating

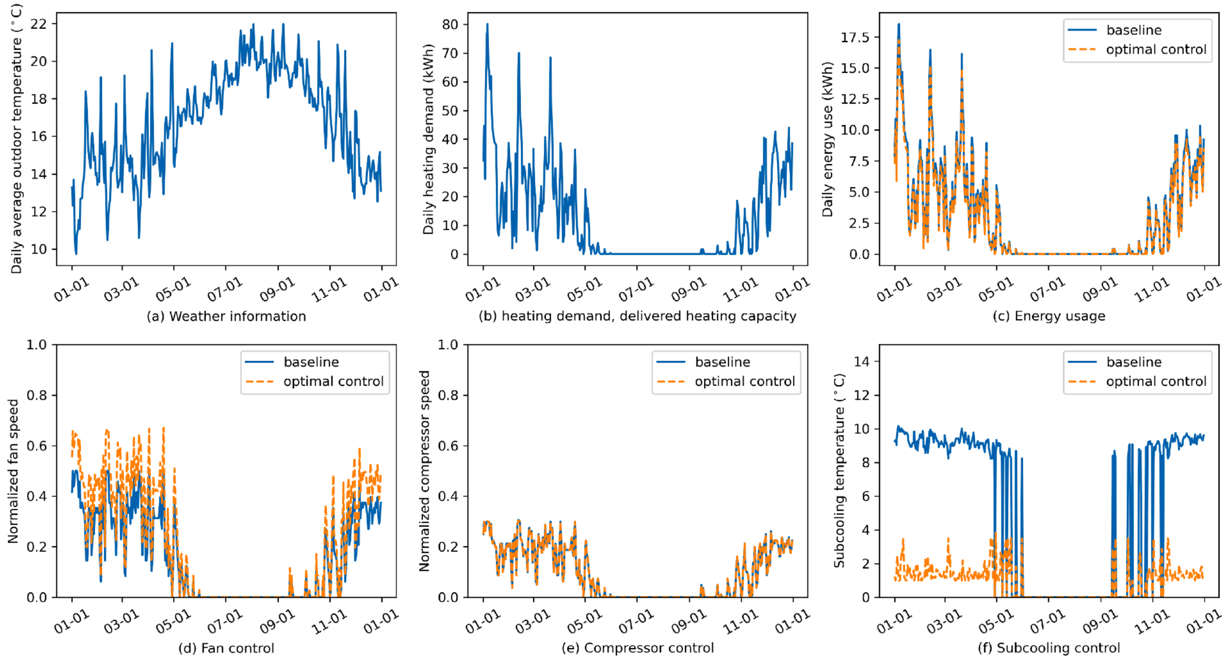

Fig. 12. Weather, heating demand, energy use, and control variables for the heat pump in Los Angeles over time.

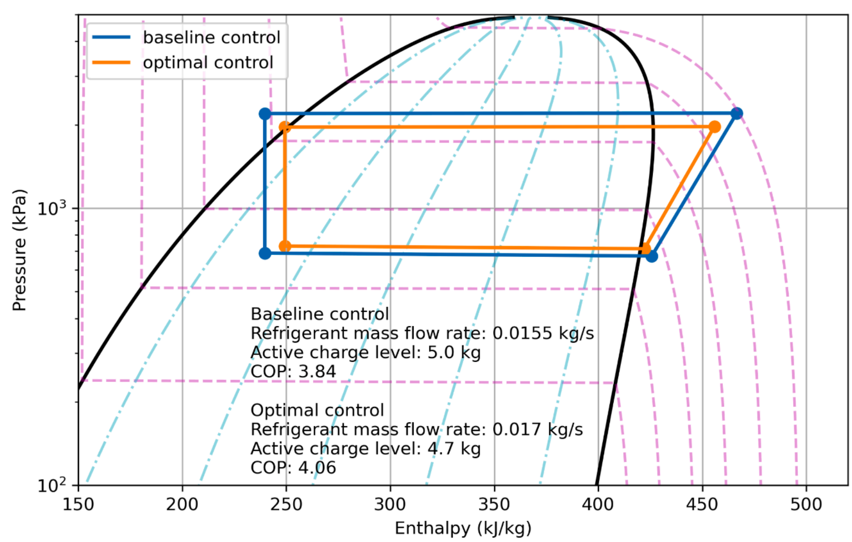

Fig. 13. Comparison of the refrigeration cycle under the baseline and the optimal control in a P-h diagram.

capacity, and the system COP increases significantly from 3.84 to 4.06 (5.7 % of increase). Note that in optimal control, the active charge level is 0.3 kg lower than the baseline, representing a 6 % decrease of charge level. This indicates that the efficiency gain can be achieved with only minor adjustments to the active refrigerant charge in the refrigeration cycle.

5. Conclusions

This study presents a novel methodology for evaluating the seasonal performance improvement of zero superheat active charge control in variable-speed heat pumps, offering significant advancements in energy efficiency. The approach begins with the development of a high-fidelity, physics-based heat pump model to simulate system performance under various control strategies. Building on this, we introduced a model-based optimal controller designed for active charge management and fan-compressor speed coordination. This controller strategically utilizes an accumulator to sustain the active charge level at zero superheat, while optimizing the EXV opening to achieve maximum COP through targeted subcooling levels. In addition, it effectively coordinates the compressor and indoor fan speeds to ensure the desired heating capacity.

Our methodology was applied across ten U.S. cities spanning different climate regions, demonstrating that the proposed optimal controller can deliver energy savings of 5.8 % to 8.0 % throughout the heating season compared to traditional superheat control with a constant charge level. The analysis attributes the COP improvement to enhanced refrigerant mass flow rate and total heat transfer coefficient, which lead to lower condensing temperatures, higher evaporating temperatures, and reduced compression pressure ratios, thereby minimizing compressor energy consumption.

This study provides crucial insights for the design and implementation of zero-superheat active charge controllers in heat pumps, addressing a gap in the market where no such control algorithm currently exists. The practical implications of this work suggest a pathway to significantly enhance heat pump efficiency and reliability. Future efforts will focus on experimentally validating the performance of the developed optimal controller and implementing a fully functional control algorithm in real-world heat pump systems.

Despite the promising results, the study has two limitations. First, the heat pump used in this study cannot operate in Climate Zones 6 and 7, which are characterized by very cold conditions. This is primarily due to the reduced efficiency and capacity of the current heat pump model under such extreme temperatures. Future work should focus on developing a cold-climate heat pump model tailored for these regions. Second, the models developed in this study are steady-state models, which may not fully address the robustness of subcooling control under transient conditions. Future research should focus on enhancing the control strategy to better handle dynamic changes and uncertainties in system operations.

CRediT authorship contribution statement

Fangzhou Guo: Writing – original draft, Validation, Methodology, Formal analysis, Conceptualization; **Donghun Kim:** Project administration, Funding acquisition; **Bo Shen:** Writing – review & editing, Software, Resources; **Philani Hlanze:** Validation, Data curation; **Jie Cai:** Writing – review & editing, Resources.

Data availability

Data will be made available on request.

Declaration of competing interest

The authors declare that they have no known competing financial interests or personal relationships that could have appeared to influence the work reported in this paper.

Acknowledgement

This research was conducted in Lawrence Berkeley National Lab as part of the U.S. Department of Energy labcall project entitled “Virtual Sensor-based FDD and Control Suite for Widespread Adoption of Residential Embedded-FDD Heat Pumps”, supported by the Assistant Secretary for Energy Efficiency and Renewable Energy, Office of Building Technologies and Industrial Efficiency and Decarbonization Office of the U.S. Department of Energy, under Contract No. DE-AC02-05CH11231.

References

[1] U. S. Energy Information Administration, Electricity data, 2020, https://www.eia.gov/energyexplained/electricity/use-of-electricity.php.
[2] J. Sim, H. Lee, J.H. Jeong, Optimal design of variable-path heat exchanger for energy efficiency improvement of air-source heat pump system, Appl. Energy 290 (2021) 116741.
[3] Z. Li, B. Shen, H. Wan, B. Fricke, Heat exchanger circuitry optimization using an enhanced integer permutation-based genetic algorithm in low-GWP reversible heat pump applications, Appl. Therm. Eng. 239 (2024) 122111.
[4] B.H. Al-Kbodi, T. Rajeh, M.E. Zayed, Y. Li, J. Zhao, J. Wu, Y. Liu, Transient heat transfer simulation, sensitivity analysis, and design optimization of shallow ground heat exchangers with hollow-finned structures for enhanced performance of ground-coupled heat pumps, Energy Build. 305 (2024) 113870.
[5] T. El Samad, Ż.-G. Alina, H. Jouhara, A.I. Sayma, A review of compressors for high temperature heat pumps, Therm. Sci. Eng. Prog. 51 (2024) 102603.
[6] B. Yu, J. Long, Y. Zhang, H. Ouyang, D. Wang, J. Shi, J. Chen, Life cycle climate performance evaluation (LCCP) of electric vehicle heat pumps using low-GWP refrigerants towards China’s carbon neutrality, Appl. Energy 353 (2024) 122061.
[7] Y. Dong, H. Yan, R. Wang, Significant thermal upgrade via cascade high temperature heat pump with low GWP working fluids, Renewable Sustainable Energy Rev. 190 (2024) 114072.
[8] C. Feng, C. Guo, J. Chen, S. Tan, Y. Jiang, Thermodynamic analysis of a dual-pressure evaporation high-temperature heat pump with low GWP zeotropic mixtures for steam generation, Energy 294 (2024) 130964.
[9] Z. Chen, Z. O’Neill, J. Wen, O. Pradhan, T. Yang, X. Lu, G. Lin, S. Miyata, S. Lee, C. Shen, et al., A review of data-driven fault detection and diagnostics for building HVAC systems, Appl. Energy 339 (2023) 121030.
[10] N. Es-Sakali, M. Cherkaoui, M.O. Mghazli, Z. Naimi, Review of predictive maintenance algorithms applied to HVAC systems, Energy Rep. 8 (2022) 1003–1012.
[11] F. Guo, B. Rasmussen, Predictive maintenance for residential air conditioning systems with smart thermostat data using modified Mann-Kendall tests, Appl. Therm. Eng. 222 (2023) 119955.
[12] Z. Li, Z. Sun, Q. Meng, Y. Wang, Y. Li, Reinforcement learning of room temperature set-point of thermal storage air-conditioning system with demand response, Energy Build. 259 (2022) 111903.
[13] S. Schmitz, K. Brucke, P. Kasturi, E. Ansari, P. Klement, Forecast-based and data-driven reinforcement learning for residential heat pump operation, Appl. Energy 371 (2024) 123688.
[14] W. Wang, Z. Zhao, Q. Zhou, Y. Qiao, F. Cao, Model predictive control for the operation of a transcritical CO2 air source heat pump water heater, Appl. Energy 300 (2021) 117339.
[15] V. Klepic, M. Wolf, T. Pröll, Extension of a low-tech model predictive control (MPC) algorithm for grid-supportive heat pump operation, Energy Build. 323 (2024) 114733.
[16] W. Chen, C. Zhijiu, Z. Ruiqi, W. Yezheng, Experimental investigation of a minimum stable superheat control system of an evaporator, Int. J. Refrig. 25 (8) (2002) 1137–1142.
[17] W. Kim, J.E. Braun, Evaluation of the impacts of refrigerant charge on air conditioner and heat pump performance, Int. J. Refrig. 35 (7) (2012) 1805–1814.
[18] J.B. Jensen, S. Skogestad, Optimal operation of simple refrigeration cycles: part i: degrees of freedom and optimality of sub-cooling, Comput. Chem. Eng. 31 (5–6) (2007) 712–721.
[19] H. Liu, J. Cai, Development of an accumulator liquid-level estimator to enable zero-superheat control and active charge management in vapor-compression systems, Int. J. Refrig. 144 (2022) 264–274.
[20] J.C. Menken, T. Weustenfeld, J. Köhler, Experimental comparison of the refrigerant reservoir position in a primary loop refrigerant cycle with optimal operation, in: 15th International Refrigeration and Air Conditioning Conference at Purdue, 2014.
[21] J.P. Koeln, A.G. Alleyne, Optimal subcooling in vapor compression systems via extremum seeking control: theory and experiments, Int. J. Refrig. 43 (2014) 14–25.
[22] S.K. Fischer, C.K. Rice, System design optimization and validation for single-speed heat pumps, ASHRAE Trans. 91 (2B) (1985) 509–523.
[23] T. Zakula, P. Armstrong, L. Norford, Optimal coordination of heat pump compressor and fan speeds and subcooling over a wide range of loads and conditions, HVAC R Res. 18 (6) (2012) 1153–1167.
[24] C.K. Rice, DOE/ORNL Heat Pump Design Model, Overview and Application to R-22 Alternatives, Technical Report, Oak Ridge National Lab (ORNL), Oak Ridge, TN (United States), 1997.
[25] R. Air-Conditioning and Heating and Institute, Positive displacement refrigerant compressors and compressor units, 2010, (ANSI/AHRI Standard 540-99).
[26] I. Brandemuehl, M. J. and Gabel, S. and Andresen, HVAC2 Toolkit, Algorithms and Subroutines for Secondary HVAC System Energy Calculations, American Society of Heating, Refrigerating and Air-Conditioning Engineers, 1993.
[27] International Code Council, 2012 International Energy Conservation Code, International Code Council, Washington, D.C., 2012.
[28] Performance rating of unitary air-conditioning & air-source heat pump equipment, 2020. AHRI Standard 210/240.
[29] U. S. Department of Energy, EnergyPlus Engineering Reference, U.S. Department of Energy, 2022. Available at: https://energyplus.net/assets/nrel_custom/pdfs/pdfs_v22.1.0/EngineeringReference.pdf.
[30] C. Booten, C. Christensen, J. Winkler, Energy Impacts of Oversized Residential Air Conditioners–Simulation Study of Retrofit Sequence Impacts, Technical Report, National Renewable Energy Lab.(NREL), Golden, CO (United States), 2014.